Supplementary Information (SI) for "Aerosol Hygroscopic Growth as a Key Driver of Aerosol-Radiation Interactions in Radiation Fog"

Hao Ding[1,2], Alejandro Baró Pérez[1,2], Nazario Mastroianni[1,2,3], Almuth Neuberger[2,3,4], Rahul Ranjan[2,3,5], Fredrik Mattsson[2,3], Liine Heikkinen[2,3], Karam Mansour[6], Stefano Decesari[6], Angelo Lupi[7], Claudia Mohr[2,3,8,9], Paul Zieger[2,3], Ilona Riipinen[2,3], and Annica M. L. Ekman[1,2]

[1]Department of Meteorology, Stockholm University, Stockholm, Sweden
[2]Bolin Centre for Climate Research, Stockholm, Sweden
[3]Department of Environmental Science, Stockholm University, Stockholm, Sweden
[4]now at: Institute for Hygiene and Environment, Hamburg State Institute for Food Safety, Health Protection and Environmental Investigations, Hamburg, Germany
[5]now at: Department of Technical Physics, Faculty of Science, Forestry and Technology, University of Eastern Finland, Kuopio, Finland
[6]Institute of Atmospheric Science and Climate, National Research Council of Italy, Bologna, Italy
[7]Institute of Polar Sciences, National Research Council of Italy, Bologna, Italy
[8]now at: Center for Energy and Environmental Sciences, Paul Scherrer Institute, Villigen, Switzerland
[9]now at: Department of Environmental Systems Science, ETH Zurich, Zurich, Switzerland

Correspondence: Hao Ding (hao.ding@misu.su.se) and Annica M. L. Ekman (annica.ekman@misu.su.se)

The supplementary information (SI) includes the wavelength-dependent complex refractive indices of the aerosol species used in MIMICA, idealized experiments with pure aerosol components, the aerosol composition used in the chemical sensitivity experiments, observations of longwave radiation at the SPC site, additional sensitivity tests examining the effects of low-level clouds, and sensitivity tests on aerosol hygroscopicity. The SI sections are organized following the order of appearance in the main manuscript.

S1 Refractive indices of aerosol species

Table S1. Wavelength-dependent complex refractive indices of aerosol species used in MIMICA. The real part (n) represents scattering, and the imaginary part (k) represents absorption component, adapted from Bond and Bergstrom (2006), Slater et al. (2020), and Baró Pérez et al. (2024).

λ (μm)	Sulfate		Black Carbon		Organic Carbon		Sea Salt		Water	
	n	k	n	k	n	k	n	k	n	k
0.230	1.450	1.000e-09	1.713	7.261e-01	1.530	5.270e-03	1.510	1.000e-05	1.377	6.400e-08
0.300	1.450	1.000e-09	1.839	7.584e-01	1.443	1.630e-02	1.510	1.000e-06	1.350	1.700e-08
0.390	1.445	1.000e-09	1.839	7.294e-01	1.530	9.750e-03	1.500	2.000e-08	1.341	3.900e-09
0.530	1.432	1.000e-09	1.850	7.213e-01	1.530	7.700e-03	1.490	1.000e-08	1.335	2.800e-09
0.700	1.427	5.200e-08	1.850	6.939e-01	1.530	1.500e-03	1.480	1.000e-07	1.331	6.800e-08
1.010	1.422	1.300e-06	1.861	7.106e-01	1.420	2.010e-02	1.470	1.000e-04	1.328	2.100e-06
1.270	1.413	7.900e-06	1.861	7.274e-01	1.420	1.770e-02	1.470	3.300e-04	1.324	1.200e-05
1.460	1.406	9.000e-05	1.869	7.397e-01	1.520	1.430e-02	1.460	5.500e-04	1.319	1.100e-04
1.780	1.393	5.100e-04	1.894	7.765e-01	1.464	6.420e-03	1.450	1.000e-03	1.312	1.200e-04
2.050	1.382	1.300e-03	1.905	7.939e-01	1.420	4.580e-03	1.450	1.500e-03	1.300	6.700e-04
2.330	1.364	2.100e-03	1.917	8.120e-01	1.510	7.330e-03	1.440	2.500e-03	1.283	6.500e-04
2.790	1.295	5.500e-02	1.936	8.510e-01	1.510	7.330e-03	1.400	8.000e-03	1.244	1.300e-01
3.460	1.361	1.400e-01	1.984	8.975e-01	1.530	2.750e-02	1.480	1.300e-02	1.423	5.000e-02
3.420	1.602	9.670e-02	1.980	8.910e-01	1.440	5.950e-03	1.484	2.060e-02	1.416	1.690e-02
4.020	1.541	3.800e-02	2.030	9.370e-01	1.460	4.880e-03	1.478	1.750e-02	1.348	4.830e-03
4.320	1.512	2.870e-02	2.040	9.460e-01	1.460	9.280e-03	1.488	2.460e-02	1.333	8.810e-03
4.620	1.489	2.250e-02	2.060	9.560e-01	1.460	1.170e-02	1.483	2.510e-02	1.327	1.510e-02
5.150	1.450	2.000e-02	2.090	9.730e-01	1.450	1.270e-02	1.459	2.880e-02	1.316	1.060e-02
6.100	1.336	3.960e-02	2.140	1.000	1.420	2.290e-02	1.505	1.800e-01	1.312	1.320e-01
6.970	0.956	2.690e-01	2.170	1.040	1.420	5.300e-02	1.450	5.430e-02	1.314	3.480e-02
7.780	1.427	1.110	2.230	1.080	1.230	6.040e-02	1.401	1.380e-02	1.295	3.470e-02
8.850	0.685	7.050e-02	2.300	1.140	2.640	3.760e-01	1.638	2.930e-02	1.264	3.920e-02
9.710	2.469	6.780e-01	2.330	1.160	1.810	4.540e-02	1.563	1.790e-02	1.230	4.810e-02
11.110	1.879	1.430e-02	2.360	1.180	1.710	4.520e-02	1.485	1.400e-02	1.149	1.070e-01
13.160	1.709	6.640e-03	2.420	1.230	1.610	5.310e-02	1.408	1.920e-02	1.171	3.170e-01
15.040	1.537	6.570e-03	2.460	1.280	1.430	1.820e-01	1.447	3.440e-02	1.283	3.950e-01
17.700	1.804	9.440e-03	2.530	1.330	2.020	1.860e-01	1.763	1.110e-01	1.401	4.280e-01
23.530	1.588	1.480e-02	2.630	1.420	1.950	2.350e-01	1.749	1.930e-01	1.524	3.920e-01
55.560	1.889	1.560e-01	2.840	1.610	1.860	4.580e-01	1.668	9.810e-01	1.689	6.180e-01

S2 Idealized experiments with pure aerosol components

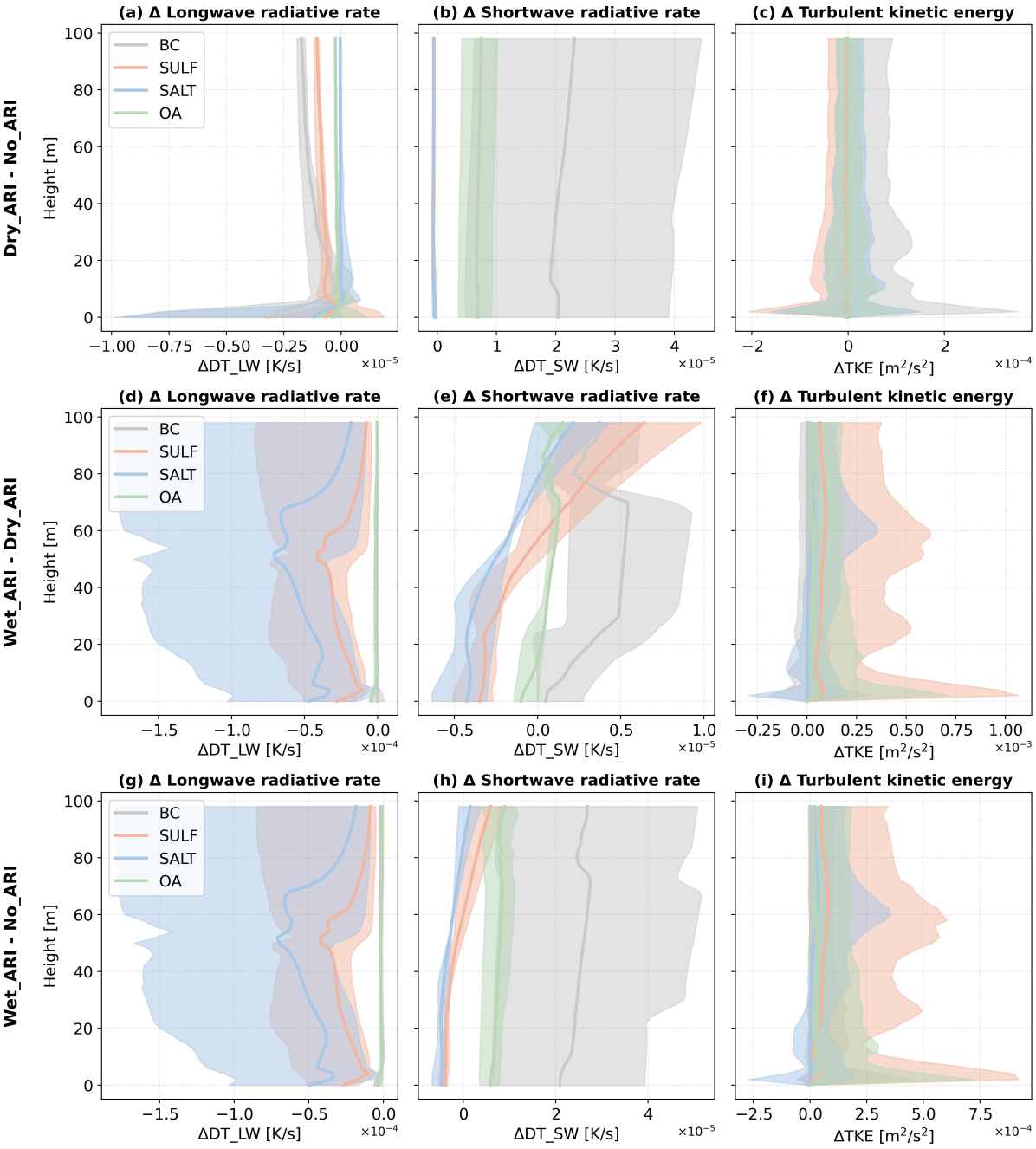


Figure S1. Vertical profiles of ARI effects driven by individual pure aerosol components (BC, SULF, SALT, and OA) in idealized experiments, derived using a differencing approach. The top, middle, and bottom panels show the dry aerosol direct effect (Pure*_DryARI−Pure*_NoARI), the radiative effect of aerosol water uptake during hygroscopic growth (Pure*_WetARI−Pure*_DryARI), and the total aerosol direct effect (Pure*_WetARI−Pure*_NoARI), respectively. The columns correspond to responses in (a, d, g) longwave radiative heating rate (DT_LW, 18 Feb 19:00–19 Feb 08:00), (b, e, h) shortwave radiative heating rate (DT_SW, 19 Feb 08:00–10:00), and (c, f, i) turbulent kinetic energy (TKE, 18 Feb 19:00–19 Feb 08:00). Solid lines denote the temporal median profiles, while shaded envelopes show the 5th–95th percentile range.

S3 Aerosol compositions in chemical sensitivity tests

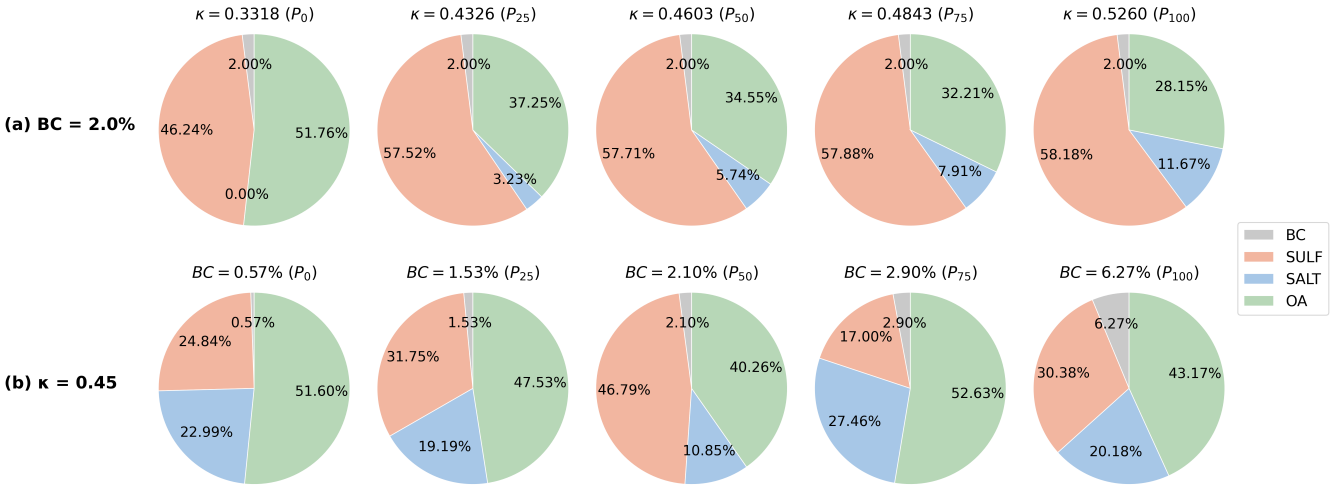


Figure S2. Aerosol chemical inputs used in the sensitivity experiments: (a) Aerosol compositions constructed from the 0th, 25th, 50th, 75th, and 100th percentiles of observed κ, with BC volume fraction fixed at the reference value of 2.0%. (b) Aerosol compositions constructed from the the 0th, 25th, 50th, 75th, and 100th percentiles of observed BC content, with κ fixed at the reference value of 0.45.

S4 Longwave radiation observations

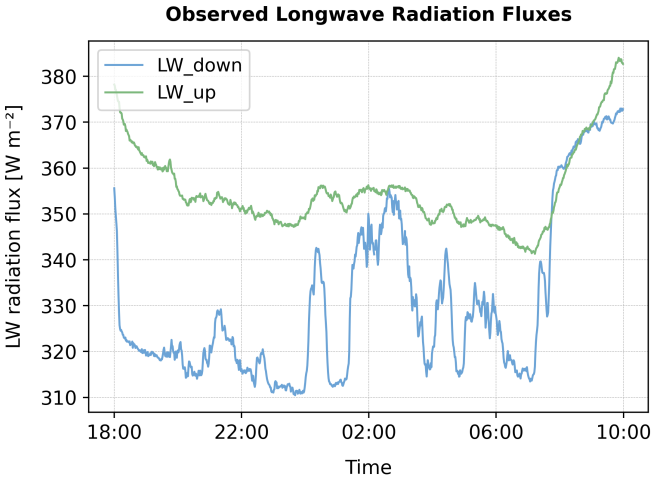


Figure S3. Time series of observed downward and upward longwave radiation fluxes at the SPC site during 18-19 February 2022.

S5 Test on low-level clouds

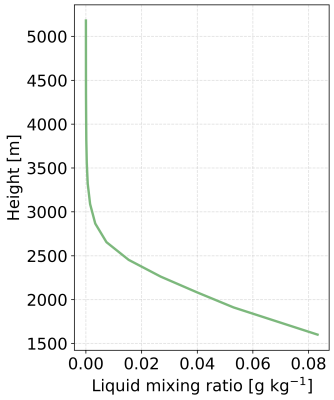


Figure S4. Initial vertical profile of liquid water mixing ratio above the model domain in the low-level cloud sensitivity experiment.

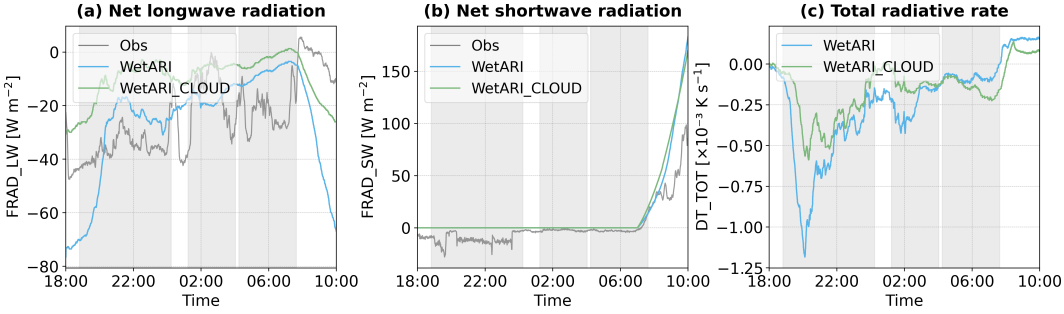


Figure S5. Near-surface time series of (a) net longwave radiation flux (FRAD_LW) and (b) net shortwave radiation flux (FRAD_SW) and (c) total radiative rate (DT_TOT) in observations (Obs) and the low-level cloud sensitivity experiment, where WetARI_CLOUD denotes the simulation with low-level clouds included.

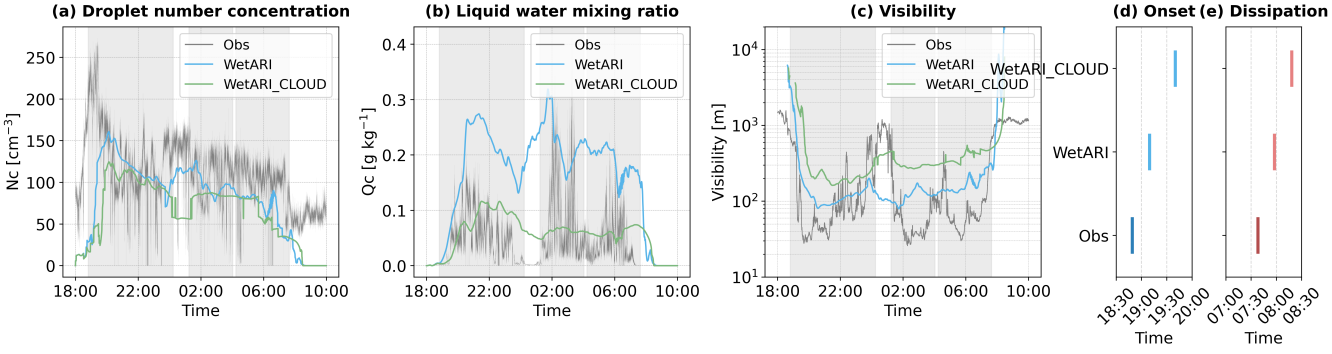


Figure S6. Near-surface time series of (a) total droplet number concentration, (b) liquid water mixing ratio, (c) visibility, (d) fog onset on Feb 18 and (e) fog dissipation time on Feb 19 in observations (Obs) and the low-level cloud sensitivity experiment, where WetARI_CLOUD denotes the simulation with low-level clouds included.

S6 Test on aerosol hygroscopicity

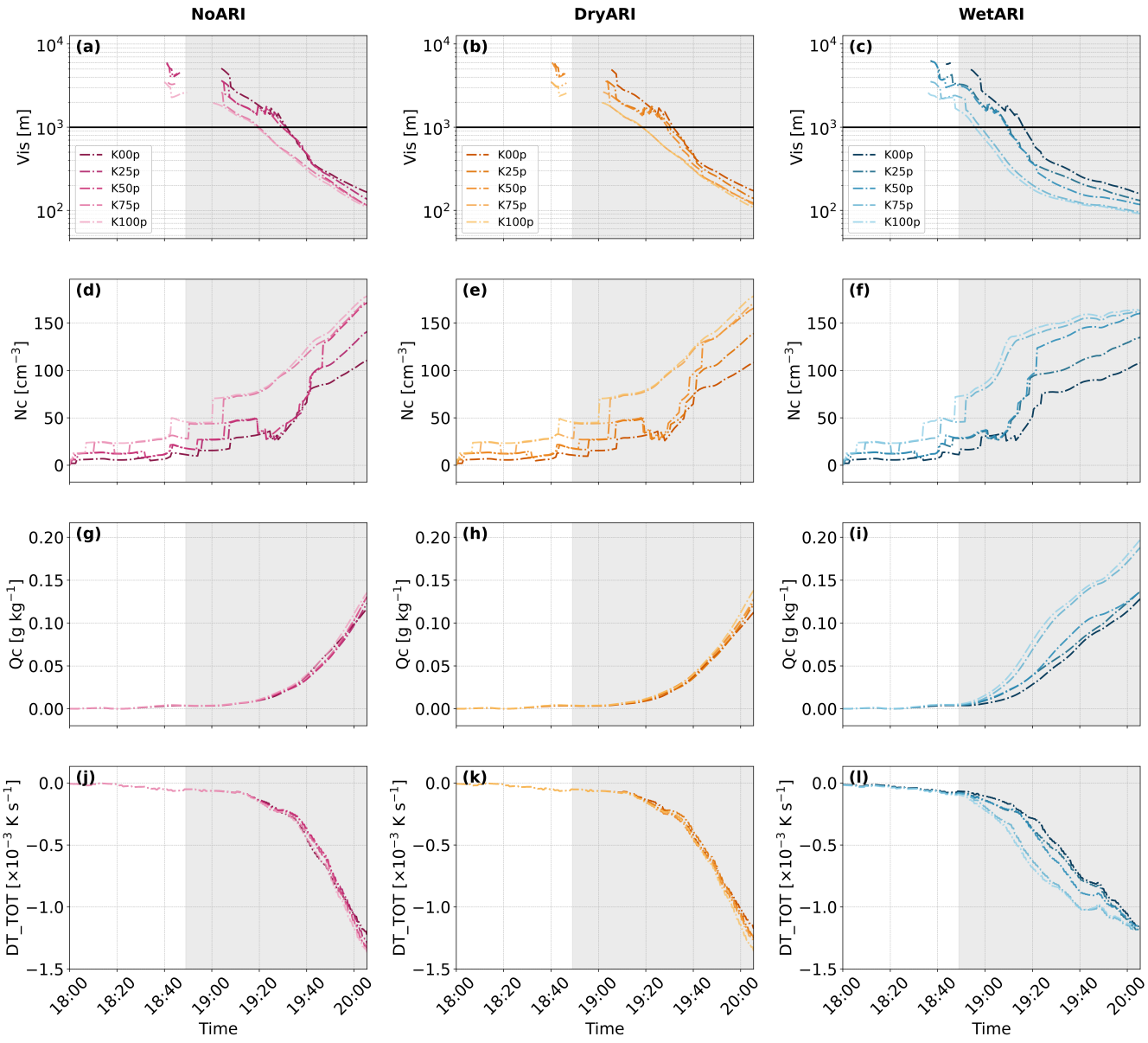


Figure S7. Temporal evolution of near-surface properties during fog formation under different κ and ARI scenarios. The columns correspond to the NoARI, DryARI, and WetARI scenarios, respectively. Darker shades correspond to lower κ. From top to bottom, the panels show (a–c) visibility (Vis), (d–f) total droplet number concentration (N_c), and (g–i) liquid water mixing ratio (Q_c), (j-l) total radiative rate (DT_TOT). Gray shading indicates the observed fog periods. Horizontal black lines in the visibility panels indicate the 1-km threshold.

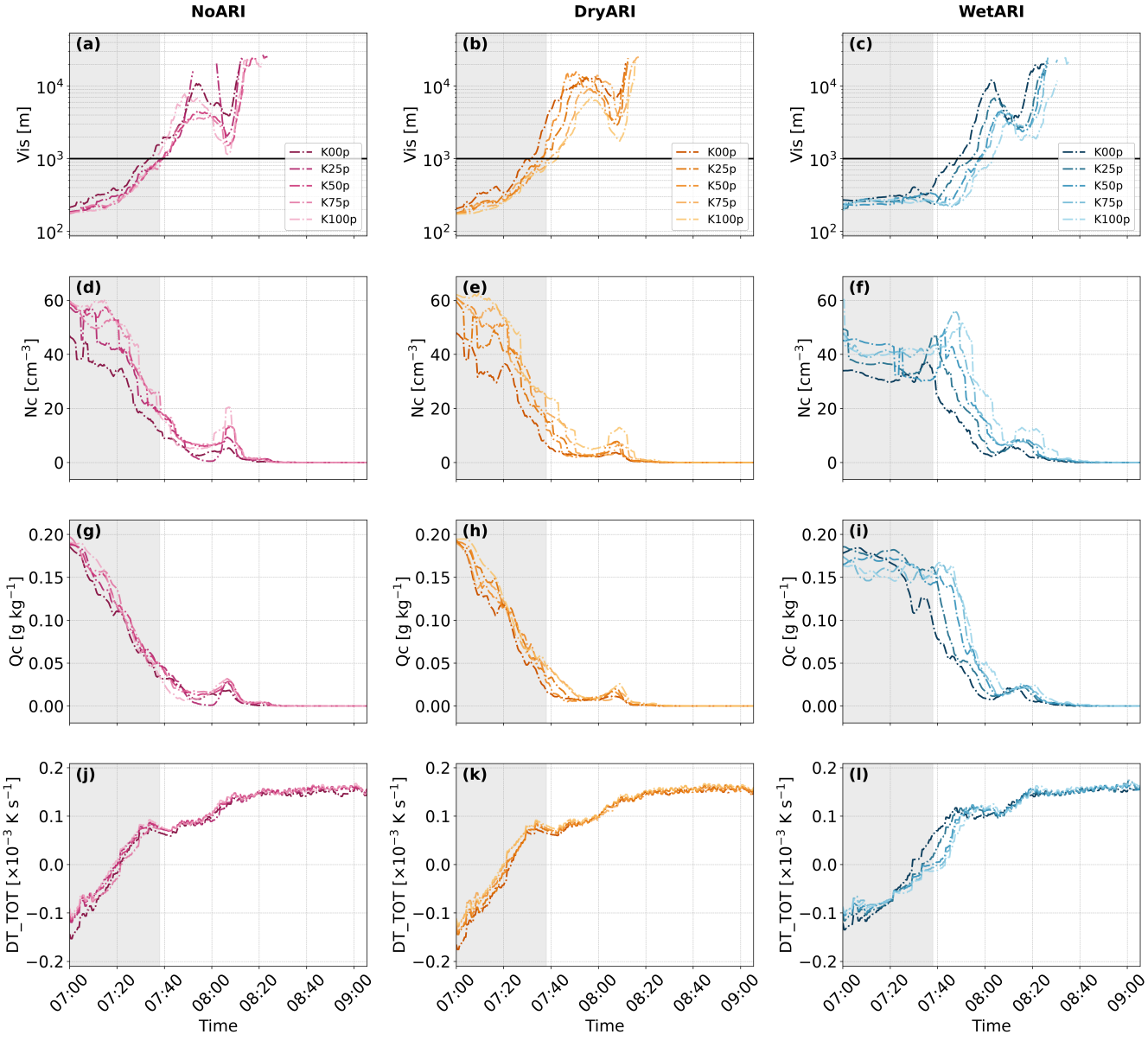


Figure S8. Temporal evolution of near-surface properties during fog dissipation under different κ and ARI scenarios. The columns correspond to the NoARI, DryARI, and WetARI scenarios, respectively. Darker shades correspond to lower κ. From top to bottom, the panels show (a–c) visibility (Vis), (d–f) total droplet number concentration (N_c), and (g–i) liquid water mixing ratio (Q_c), (j-l) total radiative rate (DT_TOT). Gray shading indicates the observed fog periods. Horizontal black lines in the visibility panels indicate the 1-km threshold.

References

Baró Pérez, A., Diamond, M. S., Bender, F. A.-M., Devasthale, A., Schwarz, M., Savre, J., Tonttila, J., Kokkola, H., Lee, H., Painemal, D., and Ekman, A. M. L.: Comparing the simulated influence of biomass burning plumes on low-level clouds over the southeastern Atlantic under varying smoke conditions, Atmospheric Chemistry and Physics, 24, 4591–4610, https://doi.org/10.5194/acp-24-4591-2024, 2024.

Bond, T. C. and Bergstrom, R. W.: Light absorption by carbonaceous particles: An investigative review, Aerosol science and technology, 40, 27–67, https://doi.org/10.1080/02786820500421521, 2006.

Slater, J., Tonttila, J., McFiggans, G., Connolly, P., Romakkaniemi, S., Kühn, T., and Coe, H.: Using a coupled large-eddy simulation–aerosol radiation model to investigate urban haze: sensitivity to aerosol loading and meteorological conditions, Atmospheric Chemistry and Physics, 20, 11 893–11 906, https://doi.org/10.5194/acp-20-11893-2020, 2020.